Computational analysis of laser cooling of ultra-cold ions in Penning traps

Dominic Meiser

Trimble Inc, Boulder, 4730 Walnut Street, Suite 201, Boulder, CO 80301, USA.

John J Bollinger

National Institute of Standards and Technology, Boulder, Colorado 80305, USA.

Abstract

We develop a computational model for the analysis of ultra-cold ions in Penning traps. We extensively verify our finite temperature model by comparison with zero temperature models and by considering well understood limiting cases. We validate the model by comparison with experimental results for single-plane to multi-plane instabilities of the ion crystal and by comparison with experimentally observed spectra for the out-of-plane modes of the ion crystal. We then use our model to study the temperature of the in-plane modes which are experimentally challenging to access. We find that ...

Findings for in-plane modes

Optimization of laser cooling parameters

Ultra-cold ions in Penning traps enable studies at the forefront of atomic physics

references

, quantum science

references

, and condensed matter physics

references

. Many of these studies benefit from colder temperatures. Colder temperatures increase the crystal stability, decrease dephasing rates, and they can increase interrogation times. Improved crystal stability has the potential to enable optical access to individual lattice sites which could lead to higher fidelity state preparation and state readout for quantum metrology

references

and quantum simulation experiments

references

.

The primary means of cooling ions in Penning traps are various forms of laser cooling including Doppler cooling and side band cooling. The basic principles of laser cooling for ultra-cold ions is the same as for neutral atoms in magneto-optical traps. But there are also significant differences that can make it challenging to understand the experimentally realized ion temperature, cooling limits, cooling and heating mechanisms, and that can make it more challenging to optimize the cooling laser parameters such as intensity and detuning as well as the cooling laser geometry.

A major difference compared to neutral atom experiments is that ions in Penning traps move in a magnetic field several Tesla strong. In steady state, the ions move along circular trajectories in this magnetic field with a frequency of a few hundred kilo Hertz for the experiments of interest to us. The rotation of the ions in the magnetic field means that the velocity of the ions periodically changes direction relative to any cooling laser beams that are stationary in the laboratory frame of reference. The typical velocity of the ions gives rise to Doppler shifts that are large in comparison with the natural line width of the ions.

A second major difference is the strong interaction between the ions due to the Coulomb force. The Coulomb force couples the ions into collective modes of motion. In contrast to the cooling dynamics of neutral atoms—which is largely a single particle phenomenon—it

is necessary to take the collective nature of the ion motion into account to fully understand the cooling dynamics of ultra-cold ions in Penning traps

Is that true?

.

To help us better understand the dynamics of ultra-cold ions in Penning traps we have developed computer simulations that allow us to quantitatively track the dynamics of the ions over time scales from fractions of a nano-second all the way to milli seconds and seconds. In this paper we demonstrate the validity of these simulations by comparison with other simulations as well as by comparison with experimental data. We then use these simulations to study the spectra of the out-of-plane and in-plane modes of motion of ultra-cold ions. We compute the temperatures of these modes and determine optimal laser cooling parameters.

Who has studied cooling dynamics before? How did they do it? Need a significant review of the existing literature here. Some key workds: Dan Dubin, Dave Wineland and JJ Bollinger, Wayne Itano, Molecular Dynamics simulations, analytical studies, fluid models, tracking codes, particle methods, PIC, Direct Simulation Mode Carlo (DSMC).

The rest of this article is organized as follows. We begin by discussing the mathematical model and computational approach underlying our analysis in section I. We then verify and validate our simulations by comparison with zero temperature models, with theoretical results, and experimental data in section II. Specifically, we compare steady state solutions and spectra for the out-of-plane modes of the ion crystal. We validate the simulations by comparison with experimental results for the single-plane to multi-plane instability. In section IV we consider the in-plane modes and in section V we present a numerical optimization of the laser cooling parameters and we discuss the coldest temperatures achievable with Doppler cooling. We wrap up with section VI

I. MODEL AND COMPUTATIONAL ALGORITHM

In this section we describe our mathematical model as well as the computational techniques on which in our numerical simulations are based.

A. Mathematical model

We treat the ions as classical point particles with velocity $\mathbf{v}_i$ and position $\mathbf{x}_i$. The motion of the ions is governed by the Hamiltonian

$$H = H_0 + \sum_{i=1}^{N} q_i \varphi(\mathbf{x}_i) \ , \tag{1}$$

where the free Hamiltonian,

$$H_0 = \sum_{i=1}^{N} \frac{1}{2m_i} \left(\mathbf{p}_i - q_i \mathbf{A}(\mathbf{x}_i)\right)^2 \ , \tag{2}$$

includes the vector potential $\mathbf{A}$ for the homogeneous axial magnetic field $\mathbf{B} = (0, 0, B_z)^T$in the Penning trap. We choose our coordinate system such that the Penning trap magnetic field $\mathbf{B} = \nabla \times \mathbf{A}$ is parallel to the z axis. With that choice of coordinate system we have $\mathbf{A} = yB_z\hat{\mathbf{x}}$ with $\hat{\mathbf{x}} = \mathbf{x}/x$ the unit vector along $\mathbf{x}$. In Eqn. (2), N is the number of ions in the trap, m_i is the mass of ion i, and q_i its charge. The electrostatic potential

$$\varphi(\mathbf{x}_i, t) = \varphi_{\text{cap}}(\mathbf{x}_i) + \varphi_{\text{wall}}(\mathbf{x}_i, t) + \sum_{\substack{j=1 \\ j\neq i}}^{N} \frac{1}{4\pi\varepsilon_0} \ \frac{q_j}{|\mathbf{x_i} - \mathbf{x_j}|} \tag{3}$$

contains the potential φ_{cap} due to the end-cap electrodes in the Penning trap, the rotating wall potential φ_{wall}, and the Coulomb potential for the interaction between the ions. In the vicinity of the ion crystal the end-cap and rotating wall potentials are well approximated by harmonic potentials. We parametrize them as

$$\varphi_{\text{cap}}(\mathbf{x}) + \varphi_{\text{wall}}(\mathbf{x}, t) = \frac{1}{2} k_z z^2 - \frac{1}{2}\left(k_x x_r^2 + k_y y_r^2\right) \tag{4}$$

where

$$k_x = \left(\frac{1}{2} + \delta\right) k_z, \qquad k_y = \left(\frac{1}{2} - \delta\right) k_z \ , \tag{5}$$

The dimensionless parameter δ characterizes the strength of the rotating wall potential. The coordinates of the ions in the rotating frame, $[x_r, y_r]^T$, are related to the laboratory frame coordinates by means of

$$\begin{bmatrix} x_r \\ y_r \end{bmatrix} = \begin{bmatrix} \cos(\vartheta(t)) & -\sin(\vartheta(t)) \\ \sin(\vartheta(t)) & \cos(\vartheta(t)) \end{bmatrix} \begin{bmatrix} x \\ y \end{bmatrix} \ . \tag{6}$$

The phase of the rotating wall potential is

$$\vartheta(t) = \omega_R t + \vartheta_0 \ . \tag{7}$$

In addition to the conservative dynamics described by the Hamiltonian the ions are subject to radiation pressure forces due the cooling lasers. We describe the radiation pressure force using a stochastic model. We discuss this model in more detail when we consider the computational integration of the equations of motion of the ions in the next section.

B. Numerical algorithm for time propagation

To numerically integrate the motion of the ions we employ a split step algorithm as is customary in e.g. molecular dynamics simulations. To advance the positions and velocities of the ions, $\{\mathbf{x}_i, \mathbf{v}_i\}$, from time t to $t + \Delta t$ we use the update formula

$$\{\mathbf{x}_i(t+\Delta t), \mathbf{v}_i(t+\Delta t)\} = U_0(\Delta t/2) U_{\text{kick}}(t+\Delta t/2; \Delta t) U_0(\Delta t/2) \{\mathbf{x}_i(t), \mathbf{v}_i(t)\} \ . \tag{8}$$

In this formula, $U_0(\Delta t/2)$ is the time evolution operator corresponding to H_0 that advances the state of the ions for a time interval of duration $\Delta t/2$. Since the free Hamiltonian contains just the kinetic energy of the ions and the Lorentz force due to the axial magnetic field the motion generated by U_0 is the well known circular Larmor precession,

$$\mathbf{x}_i(t+\Delta t/2) = \mathbf{x}_i(t) + \begin{bmatrix} s & c-1 & 0 \\ -c+1 & s & 0 \\ 0 & 0 & \omega_B \Delta t/2 \end{bmatrix} \frac{\mathbf{v}_i(t)}{\omega_B} \ , \tag{9}$$

$$\mathbf{v}_i(t+\Delta t/2) = \mathbf{v}_i(t) + \begin{bmatrix} c & -s & 0 \\ s & c & 0 \\ 0 & 0 & 0 \end{bmatrix} \mathbf{v}_i(t) \ , \tag{10}$$

where

$$s = \sin(\omega_B \Delta t/2) \tag{11}$$

and

$$c = \cos(\omega_B \Delta t/2) \tag{12}$$

with $\omega_B = B_z q/m$ the Larmor precession frequency.

The time evolution operator $U_{\rm kick}(t+\Delta t/2;\Delta t)$ corresponds to the interaction with the forces due to the electrostatic potential as well as the radiation pressure forces due to laser cooling. This operator is time dependent due to the rotating wall potential and the radiation pressure forces. We evaluate it at the mid-point of the time interval, $t+\Delta t/2$. The operator $U_{\rm kick}$ changes the momenta of the particles only,

$$U_{\rm kick}(t+\Delta t/2;\Delta t)\{\mathbf{x}_i(t),\mathbf{p}_i(t)\} = \left\{\mathbf{x}_i(t),\mathbf{p}_i(t)+\Delta t q_i \mathbf{E}(t+\Delta t/2,\mathbf{x}_i(t+\Delta t/2))+\Delta\mathbf{p}_i^{\rm laser}\right\} \ . \tag{13}$$

The kick due to the electric field is given by $\Delta t q_i \mathbf{E}(t+\Delta t/2,\mathbf{x}_i(t+\Delta t/2)) = -\Delta t q_i \nabla\varphi(\mathbf{x}_i(t+\Delta t/2))$.

Our model of laser cooling is based on resonance fluorescence for a driven two-level atom. For simplicity, we discuss our approach for a single cooling laser. For multiple cooling beams we simply compute the momentum kicks for each laser and then add them up. The photon scattering rate for a driven two-level atom is given by

$$\dot{n}(\mathbf{x},\mathbf{v}) = S(\mathbf{x})\frac{\gamma_0}{2\pi}\frac{(\gamma_0/2)^2}{(\gamma_0/2)^2(1+2S(\mathbf{x}))+\Delta^2(\mathbf{v})} \ , \tag{14}$$

where γ_0 is the natural linewidth of the cycling transition (in radians per second), $S(\mathbf{x})$ is the saturation parameter, and $\Delta(\mathbf{v}) = \Delta_0 + \mathbf{k}\cdot\mathbf{v}$ is the detuning of the cooling transition from the laser frequency including the first order Doppler shift. We assume that the atoms scatter photons with this rate with Poissonian number statistics[**?**]. We take into account the beam profile by multiplying the saturation parameter with a Gaussian factor that accounts for the spatial structure of the laser,

$$S(\mathbf{x}) = e^{-\rho^2/\sigma^2} S_0 \ , \tag{15}$$

where ρ is the distance of the atom from the center of the beam and σ is the $1/e$ radius of the intensity of the beam.

To numerically simulate laser cooling we proceed as follows. First we compute the mean number of photons scattered by ion i in time interval Δt,

$$\bar{n}_i = \dot{n}_i \Delta t \ . \tag{16}$$

The velocities and positions needed for computing $\dot{n}_j$ are taken at the center of the time step in accordance with the integration scheme discussed above. We then compute the actual number of photons scattered by each ion, n_i, as a Poissonian random number with mean $\bar{n}_i$.

Each ion receives a total momentum kick of

$$\mathbf{\Delta p}_i = \mathbf{\Delta p}_{i,\text{absorb}} + \mathbf{\Delta p}_{i,\text{emit}} \ , \tag{17}$$

where $\mathbf{\Delta p_{i,\text{absorb}}} = n_i \hbar \mathbf{k}$ and $\mathbf{\Delta p_{i,\text{emit}}}$ is the recoil corresponging to n_i photons scattered in random directions with an isotropic probability distribution. To compute $\mathbf{\Delta p_{i,\text{emit}}}$ we generate n_i vectors of length $\hbar k$ pointing in random directions. The recoil momentum $\mathbf{\Delta p}_{i,\text{emit}}$ is then obtained by adding up these vectors.

This approach captures the microscopic physics of laser cooling except for two phenomena. First, in the case of strong saturation, $S \gtrsim 1$, quantum statistical phenomena start to play a role. These manifest themselves in the form of anti-bunching of the photons scattered in resonance fluorescence. In essence, there is an anti-correlation between photon emission events due to the fact that immediately after a photon emission an atom is in the ground state with certainty and therefore cannot emitt another photon right away. The other approximation in our model is that we assume that the ion motion is uniform during an excited state lifetime, i.e. we assume that

$$\eta \equiv \gamma_0/\omega_B \ll 1 \ . \tag{18}$$

In our case this ratio is approximately $\eta \sim 0.3$.

II. VERIFICATION AND VALIDATION OF THE DYNAMICAL SIMULATIONS

In this section we verify the correctness of our numerical integration procedure. We check that the simulations converge with the expected quadratic rate as the time step size is reduced. We compare the temperature of laser cooled ions with the well known text book result for Doppler cooling. We check that the steady state obtained with a separate static zero temperature code is a steady state of our simulations. Finally, we compare simulation results for a single-plane to multi-plane instability with theoretical and experimental results.

A. Convergence

One of the most basic tests of the correctness of our time integration scheme is to verify that it converges to a solution as the time step size is reduced. To evaluate the convergence

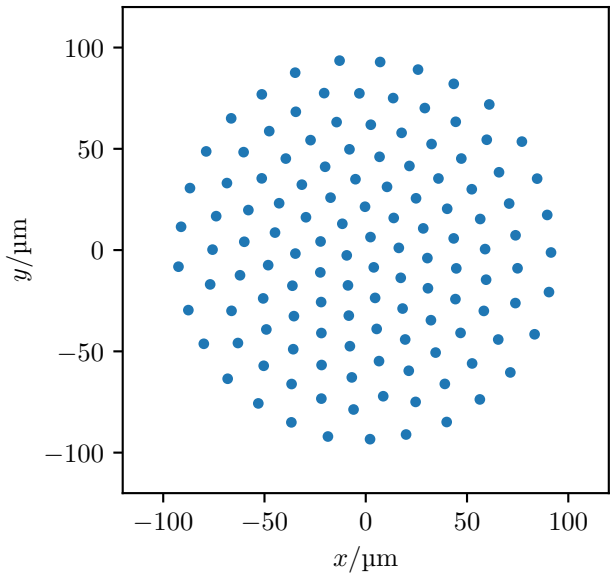

FIG. 1. Top view of steady state configuration of ions in Penning trap used for convergence study.

we initialize our simulation with a steady state configuration of 127 ions shown in Fig. 1. Here and in the results discussed below we use parameters typical for the Penning trap at NIST Boulder with a homogeneous magnetic field of $B_z = 4.4588\,\mathrm{T}$, a trap rotation frequency of $\omega_{\mathrm{trap}} = 2\pi \times 180\,\mathrm{kHz}$, end cap voltages yielding a confining potential of $k_z = 9.21\,\mathrm{MV/m^2}$, and a rotating wall potential of $V_{\mathrm{Wall}} = 1\,\mathrm{V}$ yielding $\delta = 3.5 \times 10^{-4}$.

Starting from this initial steady state configuration we integrate the equations of motion for 10 µs using different time step sizes. For each time step size we compare the final solution with a reference solution computed using a time step size of $\Delta t = 2 \times 10^{-10}\,\mathrm{s}$. We compute the error $\Delta x(\Delta t)$ in the simulation result $\mathbf{x}(\Delta t)$ as the average Euclidian distance between the reference solution $\mathbf{x}^{\mathrm{ref}} = \mathbf{x}(2.0 \times 10^{-10}\,\mathrm{s})$,

$$\Delta x(\Delta t) = \sqrt{N^{-1} \sum_{i=1}^{N} \left(\mathbf{x}_i(\Delta t) - \mathbf{x}_i^{\mathrm{ref}}\right)^2}\,. \tag{19}$$

The result is shown in Fig. 2. The error decreases quadratically for time step sizes below approximately $1.0 \times 10^{-7}\,\mathrm{s}$. At time step size of $\Delta t = 1\,\mathrm{ns}$ the mean position error of the ions is $\Delta x(1\,\mathrm{ns}) \approx 1\,\mathrm{nm}$. For reference, during this time interval the ions move on the order of 1 mm, i.e. the ion motion is integrated with a relative error on the order of 1.0×10^{-6}. For time step sizes greater than $\Delta t \approx 1.0 \times 10^{-7}\,\mathrm{s}$ the integrator hits resonances where the period of the integrator matches the period of one of the vibrational eigen modes of the

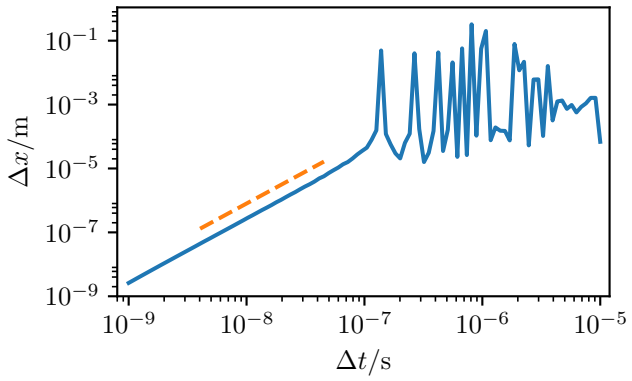

FIG. 2. Time integration errors as a function of time step size for a total time integration time of $T = 10\,\mu\text{s}$ for a typical Penning trap simulation. The dashed orange line is a quadratic for orientation. See text for details.

system. When these resonances occur the time integration errors can grow very large. While damping forces such as laser cooling can broaden the resonances and limit the growth of errors it is best to stick to time step sizes that are smaller than $\Delta t = 1.0 \times 10^{-7}\,\text{s}$. Results quoted in this paper were obtained with $\Delta t = 1\,\text{ns}$ unless noted otherwise.

B. Free space laser cooling

As a simple test of our laser cooling model we simulate free space laser cooling. Free space means that the ions are not subject to any trapping or magnetic fields. Figure 3 shows the velocities of five Beryllium ions subject to laser cooling. The atoms start with a velocity of $v_x = 10\,\text{m/s}$. The ions are irradiated by three counter propagating pairs of laser beams along the Cartesian axis $\pm\hat{\mathbf{x}}$, $\pm\hat{\mathbf{y}}$, and $\pm\hat{\mathbf{z}}$. The lasers have uniform intensities of $S = 0.1$ and are detuned by $0.5\gamma_0$ to the red of the cycling transition at 313nm. The atomic linewidth is $\gamma_0 = 2\pi \times 19\,\text{MHz}$.

As can be seen in Fig. 3, the ions are cooled to the Doppler limit. The root mean squared velocity at the Doppler temperature is

$$\sqrt{\langle v_x^2 \rangle} = \frac{\hbar\gamma_0}{m} \approx 0.87\,\text{m/s}\,, \tag{20}$$

which is in good agreement with the value of $\sqrt{\langle v_x^2 \rangle} = 1.16\,\text{m/s}$ found in our simulation.

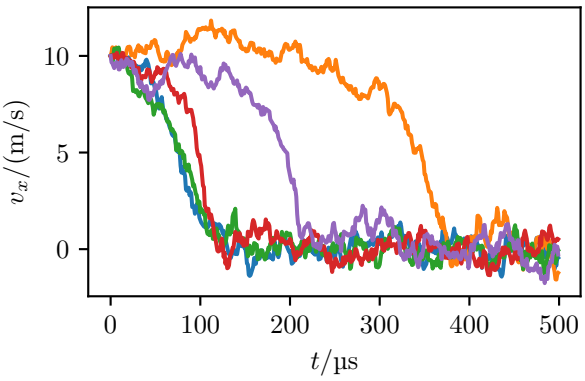

FIG. 3. Trajectories of Beryllium ions undergoing laser cooling.

C. Single-plane to multi-plane instability

When the rotation frequency of the ion crystal in the Penning trap is increased the radial confining potential generated by the axial magnetic field becomes stronger and stronger. Eventually the single plane crystal configuration shown in Fig. 1 becomes unstable and it becomes energetically favourable for the ions to arrange themselves in multiple crystal planes. The frequency at which this instability occurs is well understood theoretically

references

and has been carefully characterized experimentally

references

. We simulate the transition here to gain further confidence in the correctness and accuracy of our simulations.

To simulate the single-plane instability we start with the single plane equilibrium configuration shown in Fig. 1. We then sweep the rotation frequency of the rotating wall potential from $\omega(t = 0) = 2\pi \times 185\,\mathrm{kHz}$ to $\omega(t = 1\,\mathrm{ms}) = 2\pi \times 205\,\mathrm{kHz}$ with a constant sweep rate of $d\omega/dt = 20\,\mathrm{kHz/ms}$. After holding the rotation frequency there for 1 ms we sweep back to the original frequency with $d\omega/dt = -20\,\mathrm{kHz/ms}$. The frequency sweep $\omega(t)$ is shown in the inset in Fig. 4.

During this sweep sequence we apply an artificial damping to the ion motion in order to keep the ions close to a minimal energy configuration. The damping is given by

$$\frac{dv_z}{dt} = -\kappa_z v_z \ , \tag{21}$$

$$\frac{dv_\vartheta}{dt} = -\kappa_\vartheta \left(v_\vartheta - \omega\,|\mathbf{r}|\right) \ . \tag{22}$$

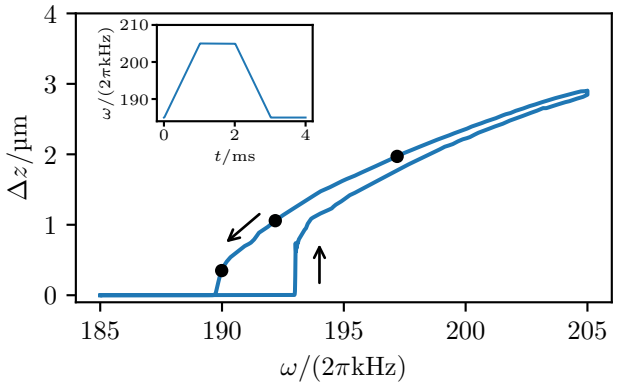

FIG. 4. Thickness of ion crystal as a function of the rotation frequency. The arrows indicate the sweep direction of the rotation frequency for the two thickness traces. The black dots indicate the rotation frequencies at which the side views in Fig. 5 are computed. The inset shows the rotation frequency as a function of time during the sweep.

For the simulations discussed here we use $\kappa_z = 1 \times 10^6\,\mathrm{s}^{-1}$ and $\kappa_\vartheta = 5 \times 10^6\,\mathrm{s}^{-1}$. We use these artificial damping terms instead of a more physically accurate laser cooling model so as to not complicate the discussion unnecessarily.

Figure 4 shows the thickness

$$\Delta z = \sqrt{N^{-1} \sum_{i=1}^{N} z_i^2} \tag{23}$$

of the ion crystal. As the rotation frequency increases the single plane configuration becomes unstable at $\omega \approx 194 \times 2\pi$kHz. The thickness of the crystal continuous to increase as more and more ions are "squeezed" out of the $z = 0$ plane.

As the rotation frequency decreases the ions move back to the $z = 0$ plane and the thickness of the crystal decreases. The thickness of the crystal lags behind the true equilibrium thickness due to the finite sweep rate. There is no bistability in this system. Eventually at $\omega \approx 190 \times 2\pi$kHz the crystal is a single plane of ions again.

Figure 5 shows a side view of the ion crystal during the down sweep of the rotation frequency. These figures illustrate the arrangement of the ions in three planes. It shows how more and more ions "fit" into the $z = 0$ crystal plane as the rotation frequency is reduced. Just above the transition frequency only a small zone around $x = y = 0$ is unstable.

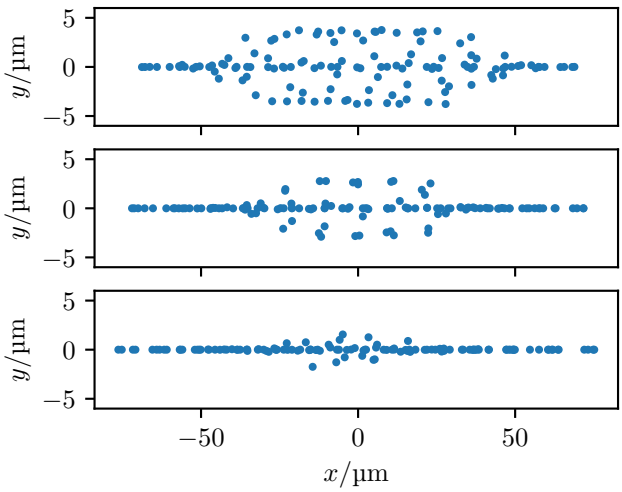

FIG. 5. Side views of ion crystal as the rotation frequency is reduced to the single plane instability frequency. The rotation frequencies at which these side views are computed are indicated by the black dots in Fig. 4.

III. FINITE TEMPERATURE MODE ANALYSIS

In this section we discuss vibrational spectra of ion crystals. We first consider the simpler out-of-plane or "drum head" modes corresponding to ion motion along the z axis. We then have a look at the more complex in-plane modes.

A. Out-of-plane modes

To compute vibrational spectra we start with the ground state configuration of Fig. 1. We then let the system evolve with Doppler laser cooling turned on for a duration of 0.1 ms. During this time the ions settle to a finite temperature steady state. We model the laser cooling generated by two counter-propagating laser beams along the $+z$ and $-z$ directions and one perpendicular laser beam parallel to x axis. The axial beams have a detuning of $\Delta = -\gamma/2$ and we assume they have a uniform intensity distribution. The perpendicular cooling beam is offset from the crystal center along the y axis by $d = 30\,\mu\text{m}$. We assume that this beam has a Gaussian intensity profile with a $1/e$ width of $\sigma = 30\,\mu\text{m}$ and a detuning of $\Delta_\perp = -\gamma/2 + dk\omega_r$. Steve et al

cite Steve's paper here

have found that this configuration should lead to a low crystal temperature corresponding

to a small multiple of the free space Doppler temperature. We assume a peak intensity of $S = 0.1$ for all three laser beams. We assume that the lasers are sufficiently broad band so that we don't have to consider interference or polarization gradient effects

Is that reasonable? Is broad band the reason we don't have to worry about interference? Are we doing lin-perp-lin for axial beams?

After the laser cooling period we turn off the cooling lasers and let the ions evolve unperturbed for another 5 ms. During this time we record the positions of the ions with a sampling rate of 0.25 µs corresponding to a Nyquist frequency of $\nu_{\text{Nyquist}} = 2\,\text{MHz}$. The total integration time of 5 ms gives us a frequency resolution of $\Delta\nu = 200\,\text{Hz}$. The power spectral density $\text{PSD}(\nu_m)$ at a discrete sampling frequency $\nu_m = m\Delta\nu$ of the motion along z is computed by

$$\text{PSD}(\nu_m) = \sum_{j=1}^{N} |\tilde{z}_j(\nu_m)|^2 + |\tilde{z}_j(-\nu_m)|^2 \ , \tag{24}$$

where

$$\tilde{z}_j(\nu_m) = \sum_{n=1}^{N_{\text{sample}}} e^{-imn/N_{\text{sample}}} z_j(n\Delta t) \tag{25}$$

Figure out best normalization to be used here. Especially with an eye towards the mode temperature discussion below.

is the discrete Fourier transform of the position of ion j.

The power spectral density is shown in Fig. 6. In that figure we also show the resonance frequencies obtained with a zero temperature code

Cite Adam+Frericks here

. As can be seen, the two spectra agree very well with one another overall. Most resonances obtained with the dynamical simulations exactly coincide with zero temperature modes. If we look closer however we see that several resonances are shifted significantly compared to the zero temperature theory. The most likely explanation is that our finite temperature initial state contains crystal defects. The crystal has switched from the ground state to some other low energy configuration during the initial equilibration period. This configuration then has a different vibrational spectrum.

Why are some modes affected by this while others aren't? Does that have to do with mode symmetries?

. Another possible explanation of the resonance shifts is that they are caused by nonlinear shifts such as the Kerr effect

Is that plausible? Only some modes shift due to symmetry? Are the level shifts in the right ball park for this to be a possible explanation?

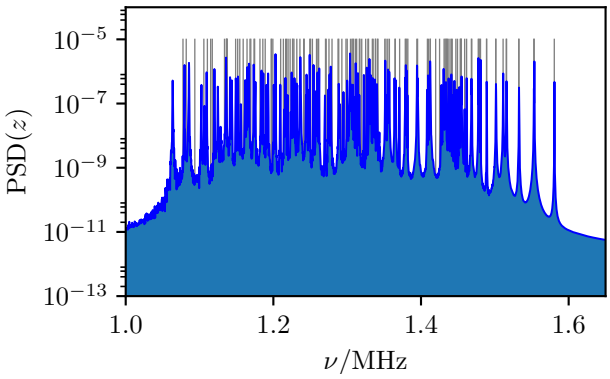

FIG. 6. Spectrum of drum head modes.

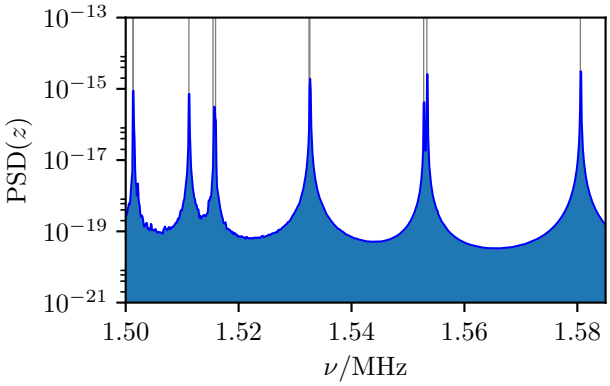

FIG. 7. Spectrum of highest few modes.

We can extract the temperature of individual modes by means of

$$T_\omega = \frac{q k_z \langle \tilde{z}_\omega^2 \rangle}{k_B} \tag{26}$$

where

$$\langle \tilde{z}_\omega^2 \rangle = \int \mathrm{PSD}(\omega) \tag{27}$$

where the integral is over a resonance and k_B is Boltzmann's constant.

Need better nomenclature here to make ω less confusing. Also need to figure out proper normalization

Make plot of $T(\omega)$.

Mode number	Mode frequency	$T_\omega/\hbar\omega$	$T_\omega/T_{\text{Doppler}}$
0	1.580 532 MHz	$1.924\,359 \times 10^2$	$3.379\,457 \times 10^1$
1	1.553 344 MHz	$1.531\,891 \times 10^2$	$2.643\,947 \times 10^1$
2	1.552 781 MHz	$2.528\,734 \times 10^1$	4.362 855
3	1.532 620 MHz	$1.033\,486 \times 10^2$	$1.759\,935 \times 10^1$
4	1.532 467 MHz	$6.318\,992 \times 10^1$	$1.075\,960 \times 10^1$
5	1.515 915 MHz	$2.115\,010 \times 10^1$	3.562 417
6	1.515 464 MHz	5.967 727	1.004 875
7	1.511 197 MHz	$4.207\,211 \times 10^1$	7.064 359
8	1.501 334 MHz	$5.175\,048 \times 10^1$	8.632 753

TABLE I. Mode temperatures of the highest few eigenmodes.

B. In-plane modes

IV. IN-PLANE MODES

V. OPTIMIZATION OF LASER COOLING PARAMETERS

VI. CONCLUSION